AMB2025-06 and AMB2025-07 Benchmark Measurements and Challenge Problems

Last updated on 2/26/2025

Modelers are invited to submit simulation results for any number of challenges they like before the deadline of 23:59 (ET) on **August 29, 2025**. Tabulated results using the challenge-specific templates are required for most challenge problems and simulation results may be submitted ambench@nist.gov. An informational webinar for AMB2025-06 and AMB2025-07 will be held on **March 13, 2025**. The webinar registration link is here. After the webinar is completed, links to the recorded presentations and to a FAQ page will be added to the **AM Bench 2025 Measurements and Challenge Problems** page. Additional information may become available later so updated versions of this document may be posted. Please check back occasionally.

All evaluations of submitted modeling results will be conducted by the AM-Bench 2025 organizing committee in conjunction with the AMB2025-06 and AMB2025-07 measurement teams. Award plaques will be awarded at the discretion of the organizing committee. Because some participants may not be able to share proprietary details of the modeling approaches used, we are not requiring such details. However, a generic description about the modeling approach and/or assumptions is requested in the challenge-specific templates. This will help the organizers with planning future benchmarks.

Please note that the challenge problems reflect only part of the validation measurement data provided by AM Bench for each set of benchmarks. The Measurement Descriptions (§3), below, describe a wider range of measurements conducted.

AMB2025-06: Arrays of adjacent laser tracks (pads) with alloy 718 material with two pad geometries and three scenarios: (1) bare plate, no powder layer, (2) 80 µm powder layer on plate, and (3) 160 µm powder layer on plate. Detailed descriptions are found below, and simulation results may be submitted to ambench@nist.gov.

Challenges

- Pad Melt Pool Geometry (CHAL-AMB2025-06-PMPG): Laser track geometrical measurements (depth, width, etc.) describing the overlapping laser tracks at specified locations of all pads. Additional metrics include the total solidified area above the substrate and the total dilution area below the substrate.
- Pad Surface Topography (CHAL-AMB2025-06-PST): Surface roughness and fused layer thickness measurements for different regions of the pads.

AMB2025-07: Arrays of adjacent laser tracks (pads) with alloy 718 material with two pad geometries and two laser turnaround (i.e., skywriting) times. These experiments were bare plates with no powder. Detailed descriptions are found below, and simulation results may be submitted to ambench@nist.gov.

Challenges

- Pad Cooling Rate and Time Above Melting (CHAL-AMB2025-07-PCRTAM): Cooling rate immediately following complete solidification (below solidus) at specified locations within pads. Time above the midpoint between the solidus and liquidus temperatures for the melt pool at

specified locations within pads. This metric is closely related to melt pool length but is explicitly location specific.

- Pad Melt Pool Geometry (CHAL-AMB2025-07-PMPG): Laser track geometrical measurements (depth, width, etc.) describing the overlapping laser tracks at specified locations of all pads. In addition, the final track melt pool shape for all pads.

Contents

1 Overview and Basic Objectives

The AMB2025-06 and AMB2025-07 benchmarks explore a range of 2D arrays of laser tracks on solid metal IN718 plates and single layers of IN718 powder on solid metal IN718 plates. The primary laser parameters such as laser power, speed, and spot diameter, and hatch spacing were fixed. The pad geometry, laser turnaround time (i.e., skywriting time), and powder layer thickness were the investigated variables. In situ measurements include location-specific liquid and solid cooling rates, and location specific time above melting. Ex situ measurements include 2.5D topography of the solidified laser tracks and cross-sectional geometry and microstructure measurements. The same sets of in situ and ex situ measurements were performed for AMB2025-06 and AMB2025-07 benchmarks. Additionally, these challenges share the same pad geometry and have one shared condition (laser turnaround time = 0.75 ms, bare plate) so they are described in a single document. A summary of these two experiment sets is shown in the Table 1.

Table 1. AMB2025-06 and AMB2025-07 unique variables. Each experiment includes 5 mm × 5 mm and 1 mm × 5 mm pad geometries.

AM Bench Challenge Number	Laser turnaround times (ms)	Powder Layers (µm)
06	0.75	0 (bare plate), 80, 160
07	0.75, 5.0	0 (bare plate)

2 Sample, Laser Processing, Machine and Monitoring Setup

2.1 Plate preparation

Sample substrates were cut from a rolled and annealed IN718 sheet. The material certificate for the as-received IN718 sheet is available in the calibration dataset (see §**Error! Reference source not found.**). The following steps were taken to prepare the samples:

- 3.17 mm (1/8”) thick IN718 sheet was cut to produce 25.4 mm x 25.4 mm (1” × 1”) bare plates.
- The bare plates were random-orientation ground with 120 grit SiC paper. The resulting surface roughness was Sa = 0.3 µm ± 0.1 µm measured by focus variation.

2.2 Powder layer

IN718 powder was used from a single lot (Lot number K201801). The particle size distribution (PSD) was measured via dynamic image analysis (DIA). The minimum chord length ($X_{c,\min}$) and equivalent circular area diameter (X_{area}) from DIA and the vendor supplied spherical diameter values from laser diffraction are provided in Table 2. The values are the average of three measurements, and the bounds are 95% confidence intervals. Other powder properties include the vendor supplied apparent density (4.05 g/cm³, which was measured according to ASTM B417) and the vendor supplied chemical composition provided in Table 3. No uncertainty was provided for the chemical composition measurements. As an

approximation for the measurement variation, we recommend using the check analysis tolerances provided in ASTM F3055 (Standard Specification for Additive Manufacturing Nickel Alloy (UNS N07718) with Powder Bed Fusion) [1]. The powder size measurements and vender supplied specification sheet are provided in the calibration dataset (see §5).

Table 2. Powder size distribution measurements. Dynamic Image Analysis results are the average ± 95% confidence interval (n = 3).

Measurement	D10 (µm)	D50 (µm)	D90 (µm)
Dynamic Image Analysis, $X_{c,min}$	16.8 ± 0.2	28.6 ± 0.6	47.9 ± 1.0
Dynamic Image Analysis, X_{area}	17.9 ± 0.3	31.0 ± 0.7	52.2 ± 0.5
Vendor supplied, Laser diffraction ISO13320	17.53	31.98	53.79

Table 3. Vendor supplied, powder chemical composition (see vendor supplied powder certificate in calibration dataset, §5, for more details). Composition ranges are based on ASTM F3055-14a [1].

Fe **Rem.**	**Ni** **50.00-55.00**	**Cr** **17.00-21.00**	**Nb** *	**Mo** **2.80-3.30**	**Ti** **0.65-1.15**	**Al** **0.20-0.80**	**Co** **≤ 1.0**
Balance	53.48	18.40	5.48	3.01	1.00	0.48	0.02
Cu **≤ 0.3**	**Si** **≤ 0.35**	**Mn** **≤ 0.35**	**Ta** *	**C** **≤0.08**	**S** **≤ 0.015**	**P** **≤ 0.015**	**B** **≤ 0.006**
< 0.01	0.03	< 0.01	< 0.01	0.05	< 0.005	< 0.010	0.003
Ag	**Pb**	**Se**	**Bi**	**O**	**N**	**H**	
< 0.0001	< 0.0001	< 0.0001	< 0.0003	0.014	0.011	0.0006	

* Nb + Ta should be between 4.75 and 5.50 % wt.

Powder layers were created using polyethylene terephthalate (PET) tape with silicon adhesive acting as shims attached to the substrates. Powder was placed on the substrate and leveled by hand using a single edge, carbon steel razor blade advanced across the shims. The razor blade was held at an acute angle, roughly 45°, with respect to the substrate on the side corresponding to the advancing direction of the razor blade (see Figure 1). The spread layer was deemed satisfactory if it appeared uniform without streaks or skips and the shims were virtually free of powder. Figure 2 shows representative images of the powder layers that were taken after the plates were placed inside the machine for laser scanning. The tape thickness was measured with a micrometer to be nominally 80 µm. A double layer of tape was used to double the layer thickness to nominally 160 µm. The thickness uncertainty is estimated as ± 5 µm (Type B, p = 95 %). Keyence point scan measurements indicated a height difference between the spread layer and the starting base plate of 60 µm and 140 µm for the 80 µm and 160 µm shims, respectively. We interpret these measurements to measure an average height (sampling the peaks of powder particles and the valleys between particles); hence, the measurements are less than the maximum height or shim thicknesses. The powder layer thickness is typically defined by the gap between the recoating plane (i.e., the plane of the razor blade set by the shims) and the reference surface below the powder (i.e., the bare plate). Therefore, the powder layer thickness will be defined by

the shim thickness rather than an average surface height or other direct measurement on the powder layer itself.

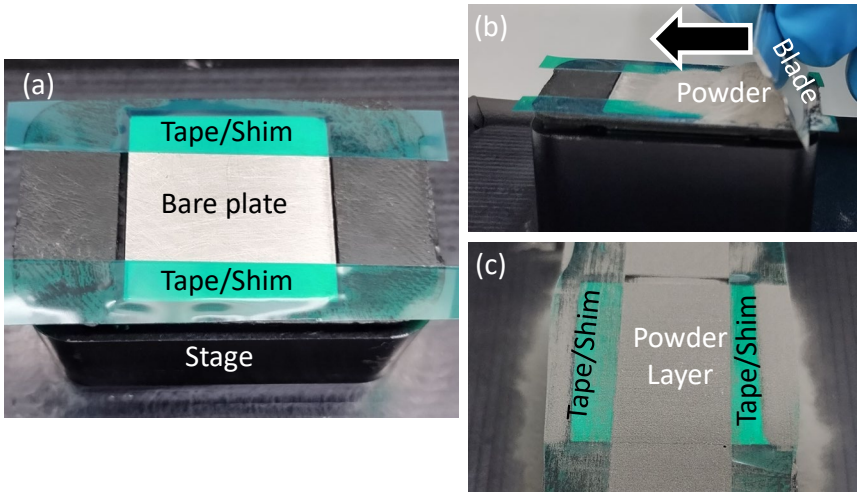

Figure 1. (a) bare plate with tape shims, (b) powder heap that is leveled with a razor blade moved across the shims, and (c) resultant powder layer on bare plate.

Typical images of the powder layers were collected and are available as part of the calibration data set (§5). Three repeat spreads and images are provided for each powder layer thickness. A single image for each powder layer thickness is show in Figure 2.

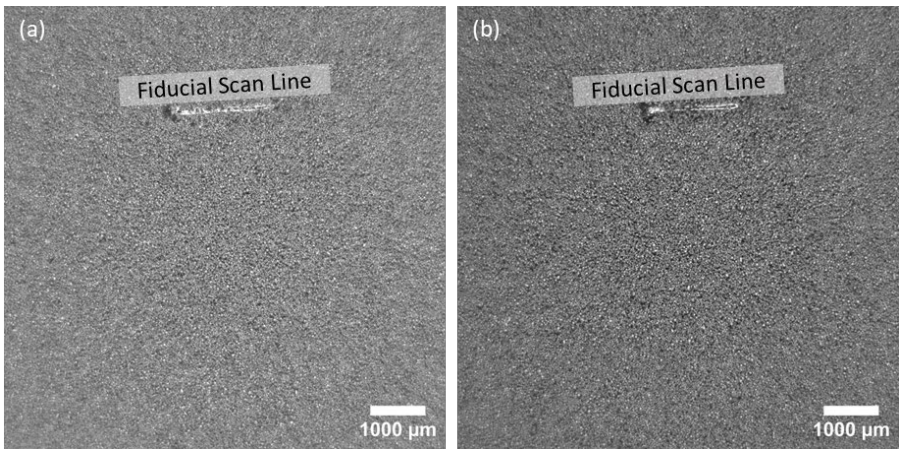

Figure 2. Images of spread powder layer (a) 80 µm and (b) 160 µm. A fiducial scan line in the images was created with the laser after the powder layer was spread.

2.3 Laser processing parameters

2.3.1 FLaMI Testbed Performance

All individual laser tracks and pads were produced using the Fundamentals of Laser-Material Interaction (FLaMI), which is a NIST-designed and built laser-processing metrology platform. A separate publication

describes the machine characterization in detail [2]. A summary of the machine and the performance is given here.

The machine was configured with a Yb-doped fiber laser with a central wavelength of 1070 nm, maximum output of 500 W, and a spot size (gaussian diameter) of 72 µm ± 3.5 µm for the experiments in this work. The gaussian diameter refers to the result of a regression analysis to the power profile using a 2-dimensional gaussian curve fit. For a perfect gaussian power profile distribution this is equivalent to D4σ. The performance of the testbed is provided in Table 4. Beam diameter measurements over the range of ± 3 mm of the beam waist are provided in Ref. [2].

Table 4. Summary of the FLaMI testbed performance [2]. Meas. Unc. = measurement uncertainties.

Measurand	**Measurement results**	**Description**	**Operation range**
Laser power	±2.5 %	Meas. Unc. Type B, k = 1	70 W to 1000 W
Laser power stability	±1 %	Std. dev.	-
Laser power rise/fall time	< 40 µs	-	-
Gaussian beam diameter	±4.8 %	Meas. Unc. at beam waist, Type A, k = 1	72 µm in this study, approx. 50 µm to ≥125 µm with different collimators
Beam waist position	105 µm	Max. dev.	-
Positioning and trajectory accuracy	41 µm	Max. dev.	-
	±21 µm	RMSE	-
Jump speed	≥ 0.75 ms	Jump speed with 110 µm hatch spacing with 960 mm/s scan speed	-
Scanning speed accuracy	± 0.6 %	Meas. Unc. Type B, k = 1	< 14 m/s with a single track* < 2 m/s with a pad**
Oxygen content	< 500 ppm	-	-
Gas flow speed	±10 %	Meas. Unc. Type B, k = 1, with argon	< 5.5 m/s at 5 mm above the build plane

*Tested for single tracks only

**Maximum speed tested for raster-scanned pads with 110 µm hatch spacing

2.3.2 Single laser tracks

Single track laser scans on bare plates of IN718 were performed to generate calibration data. The laser power, laser scan speed, and spot diameter (Dg = gaussian diameter) were 285 W, 960 mm/s, and 72 µm, respectively. The track length was approximately 8 mm, and they were cross sectioned approximately in the middle of the track length. Both halves of the plate were metallographically prepared and etched to reveal the solidified melt pool. This resulted in 6 melt pool measurements from 3 repeat laser tracks. Figure 3 shows a top view of the laser tracks along with an exemplar cross-sectional micrograph and segmented melt pool.

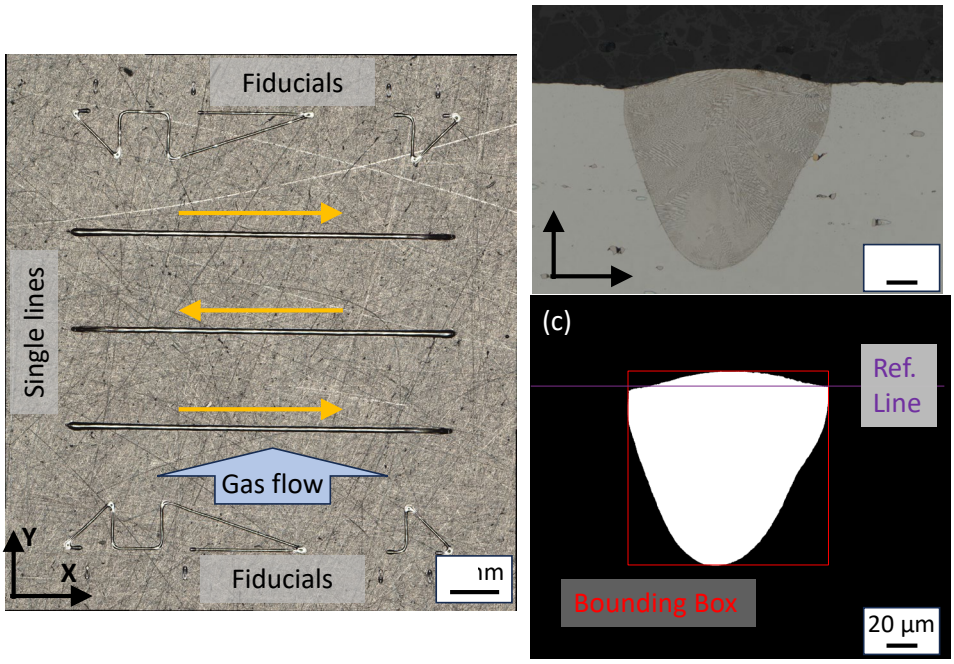

Figure 3. (a) top view of single track, bare plate laser scans (b) cross-sectional micrograph of single track, (c) segmented image of melt pool showing the surface reference line (Ref. Line) and the bounding box measurement.

Melt pool measurements were made using the Segment Anything Model (SAM) [3] in MATLAB (R2024a) and by hand using ImageJ (1.54f). A horizontal reference line at the plate surface was drawn by hand. The melt pool horizontal and vertical distances are defined by a bounding box. The width of the melt pool is the box width. The total vertical distance of the melt pool is the box height. The box height can be broken into the melt pool above the surface reference line (bead height) and below the surface reference line (depth). For segmentation, a small amount of cleanup of the mask was done by hand. An example mask is shown in Figure 3c. The measurement results are provided in Table 5.

Table 5. Single track, cross-sectional melt pool measurements. The combined expanded uncertainty (U) follows the same uncertainty calculations as outlined in Ref. [4] for single track, bare plate measurements. An uncertainty budget for image segmentation results was not calculated.

	Hand Measurements				Image Segmentation				
	Box Width (µm)	Box Height (µm)	Bead Height (µm)	Depth (µm)	Box Width (µm)	Box Height (µm)	Bead Height (µm)	Depth (µm)	Melt Pool Area (µm²)
1	135.4	133.8	9.7	124.2	135.3	133.6	9.8	123.9	12661
2	138.0	136.9	11.0	125.8	138.4	137.4	11.4	126.1	13048
3	137.4	136.6	10.7	125.9	137.0	136.6	10.9	125.7	12938
4	137.8	133.0	10.1	122.9	137.0	132.9	10.3	122.6	12781
5	140.6	135.6	10.7	124.9	139.9	135.8	10.9	124.9	13096
6	137.6	136.8	10.1	126.7	136.9	136.7	10.2	126.5	13155
Average	137.8	135.5	10.4	125.1	137.4	135.5	10.6	124.9	12946
Std. Dev.	1.7	1.7	0.5	1.4	1.6	1.8	0.6	1.5	193
U (k=2)	5.9	13.7	1.7	12.6	n/a	n/a	n/a	n/a	n/a

2.3.3 Laser pads

Two-dimensional arrays (pads) were created using the processing conditions listed in Table 6. The laser position versus time was measured using non-melting tests with high-speed imaging (see §5 for calibration data). Participants may request an XY2100 type scan file, although the FLaMI machine does not use this type of input file. Alternatively, the laser scan strategy is described in Figure 4 for the 5 mm × 5 mm pad with a laser turnaround time of 0.75 ms. Note the beam offset so that the melted material remains within the prescribed geometry. The same strategy was used for the 5 mm × 1 mm pad with the total pad width of 1 mm. The 5 ms laser turnaround time experiments used the same strategy with Δt = 5 ms instead of 0.75 ms. No image of the pads is provided so that hints cannot be gleaned for the behavior associated with challenge measurands.

Table 6: FLaMI processing conditions

Base laser processing conditions	
Laser power	285 W
Laser speed	960 mm/s
Pad hatch spacing	0.11 mm
Laser spot size (gaussian)	72 µm
Laser energy distribution	Circular, gaussian
Scan strategy	± X-direction
Pad geometries	5 mm × 5 mm, 1 mm × 5 mm
Inert gas	Argon
Max. Oxygen level	330 ppm
Gas flow speed (Z = 5 mm)	3.7 m/s
Gas flow direction	Positive Y-direction
Chamber pressure	Atmospheric (101 kPa)
Substrate and chamber temperature	Room temperature (22 °C)
Laser incidence angle range (see Figure 6)	5° ± 0.5°

Substrate	IN718 Ground plate
Powder layer thickness	Variable (see Table 1)
Laser turnaround time	Variable (see Table 1)

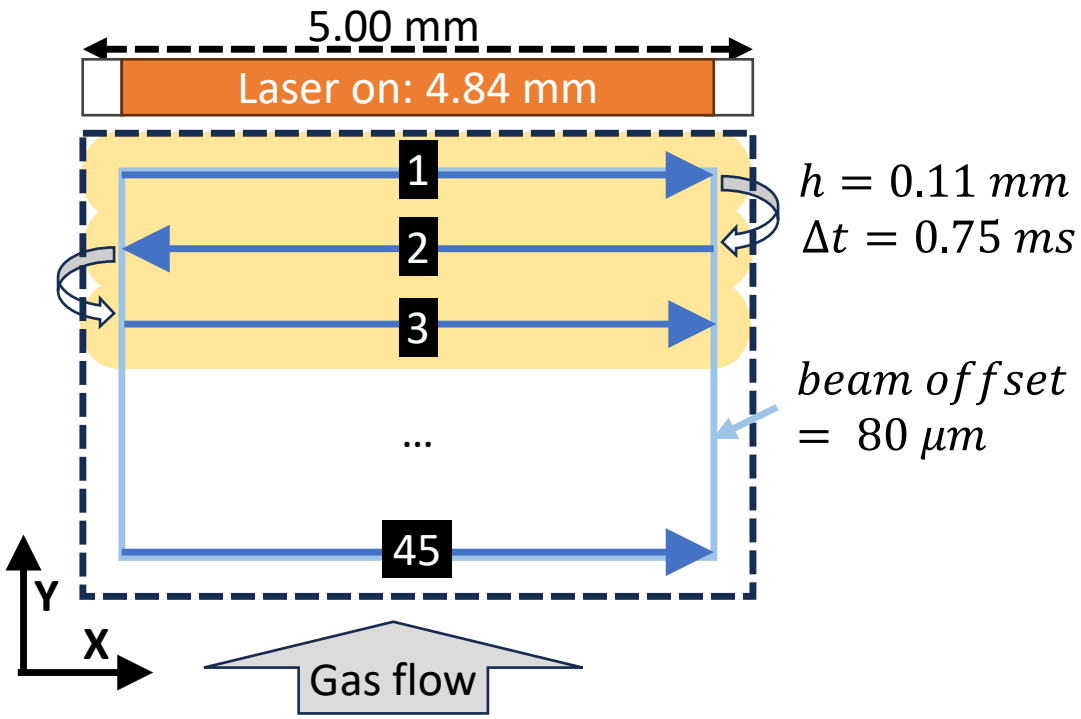

Figure 4. Illustration of laser scan strategy for 5 mm × 5 mm pad with a 0.75 ms laser turnaround time.

2.4 Gas flow system

The build chamber environment (< 18 L) is controlled by flowing inert gas through an inlet and outlet (Figure 5a). The chamber is not tightly sealed so the mass flow rate on the inlet is set higher than the outlet to maintain a low oxygen environment. The oxygen level is measured on the outlet. The directional gas flow is primarily in the positive Y-direction. The chamber is always centered about the sample. The gas flow speed was measured using a single direction hot-wire anemometer. The speed profile at the center position is shown in Figure 5b.

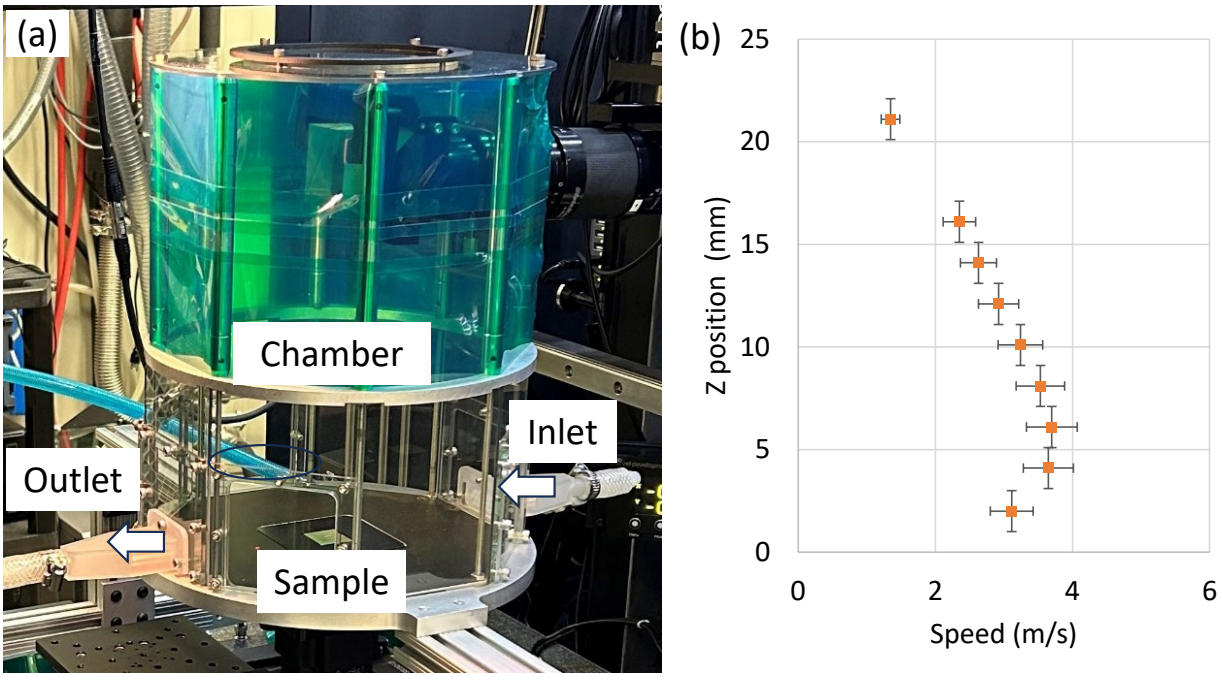

Figure 5. (a) photograph of build chamber (b) argon gas flow profiles measured at the center position of the sample with 0.83 L/s inlet flow rate. Z position = 0 mm is the sample surface. Horizontal error bars are the standard uncertainty of the measured flow speed, and vertical bars are the positioning uncertainty of the anemometer positioning stage [2].

2.5 Thermography

High-speed, staring thermography was obtained with the camera and settings given in Table 7. A mirror was used so that the imaging results in a top-down view (approximately normal to the sample) of the process as shown in Figure 6. Temperature calibration and non-uniformity correction were performed with a high temperature black body furnace.

Table 7: Camera properties for high-speed staring thermography camera.

Sensor Type:	Complementary metal-oxide semiconductor (CMOS)
View Angle:	< 2° off-normal
Wavelengths:	800 nm to 900 nm
Magnification:	14.3 µm/pixel
Window Size (x by y):	640 pixels × 480 pixels
iFoV (x by y)	9.16 mm × 6.87 mm
FoV (x by y)	9.16 mm × 6.87 mm
Frame Rate	48 kHz
Integration Time	19.0 µs
Bit depth:	12-bit
Calibrated Temperature Range:	850 °C to 1200 °C

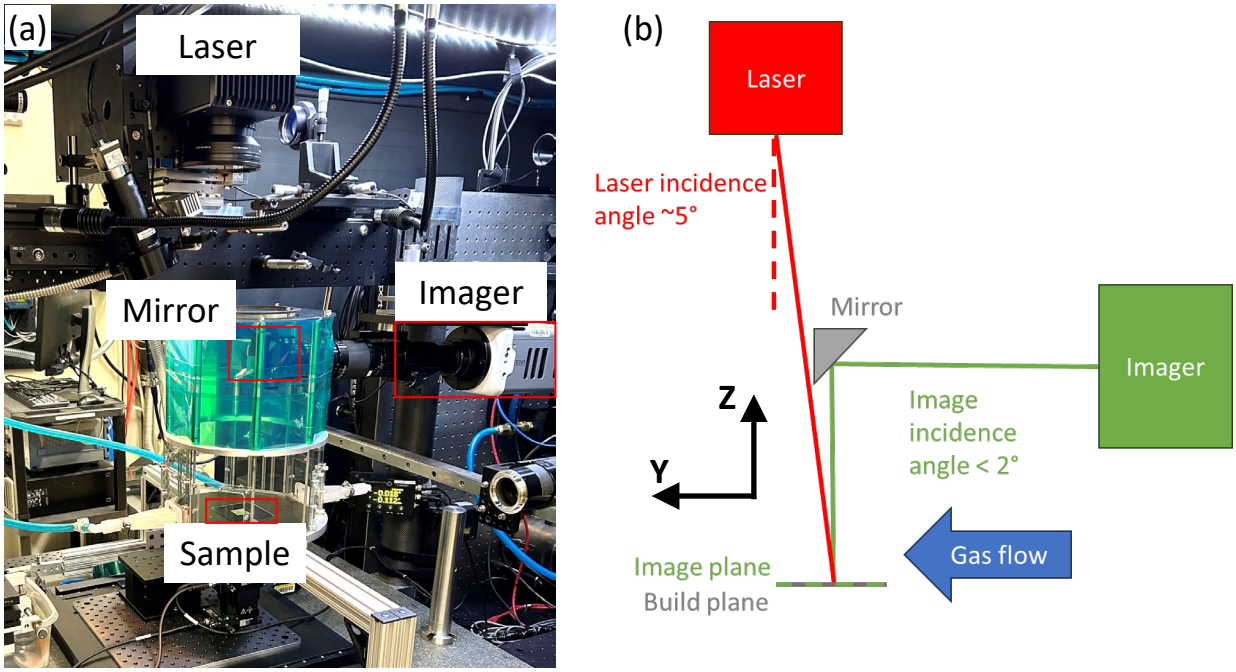

Figure 6. (a) Photograph and (b) schematic of thermography measurement setup.

2.6 Specimen naming convention

The AMB2025-06 and AMB2025-07 specimens use the following naming convention. The file name structure is date_AMB_T#2_P#. The # in T#2 goes from 1 to 12 representing the 12 plates (3 repeats for 4 conditions). The # in P# goes from 1 to 3 representing the pieces after sectioning. Measurements prior to cross-sectioning (i.e., in-situ or surface topography) will not have a P# suffix.

Table 8. Complete list of samples and main variables. Cross-section position uncertainty is estimated at ± 0.075 mm.

	Laser turnaround time (ms)	Powder layer thickness (µm)	Pad Width (mm)	Cross-section Position (mm)
20241010_AMB_SL	n/a	0	Single tracks	n/a
20241010_AMB_T12_P1	0.75	80	5	0.460
20241010_AMB_T12_P2	0.75	80	5	2.545
20241010_AMB_T12_P3	0.75	80	1	0.556
20241015_AMB_T22_P1	0.75	80	5	0.460
20241015_AMB_T22_P2	0.75	80	5	2.545
20241015_AMB_T22_P3	0.75	80	1	0.556
20241015_AMB_T32_P1	0.75	80	5	0.460
20241015_AMB_T32_P2	0.75	80	5	2.545
20241015_AMB_T32_P3	0.75	80	1	0.556
20241010_AMB_T42_P1	0.75	160	5	0.460
20241010_AMB_T42_P2	0.75	160	5	2.545
20241010_AMB_T42_P3	0.75	160	1	0.556
20241015_AMB_T52_P1	0.75	160	5	0.460
20241015_AMB_T52_P2	0.75	160	5	2.545

20241015_AMB_T52_P3	0.75	160	1	0.556
20241015_AMB_T62_P1	0.75	160	5	0.460
20241015_AMB_T62_P2	0.75	160	5	2.545
20241015_AMB_T62_P3	0.75	160	1	0.556
20241010_AMB_T72_P1	0.75	0	5	0.460
20241010_AMB_T72_P2	0.75	0	5	2.545
20241010_AMB_T72_P3	0.75	0	1	0.556
20241015_AMB_T82_P1	0.75	0	5	0.460
20241015_AMB_T82_P2	0.75	0	5	2.545
20241015_AMB_T82_P3	0.75	0	1	0.556
20241015_AMB_T92_P1	0.75	0	5	0.460
20241015_AMB_T92_P2	0.75	0	5	2.545
20241015_AMB_T92_P3	0.75	0	1	0.556
20241010_AMB_T102_P1	5	0	5	0.460
20241010_AMB_T102_P2	5	0	5	2.545
20241010_AMB_T102_P3	5	0	1	0.556
20241010_AMB_T112_P1	5	0	5	0.460
20241010_AMB_T112_P2	5	0	5	2.545
20241010_AMB_T112_P3	5	0	1	0.556
20241010_AMB_T122_P1	5	0	5	0.460
20241010_AMB_T122_P2	5	0	5	2.545
20241010_AMB_T122_P3	5	0	1	0.556

3 Measurement Descriptions

The AMB2025-06 and AMB2025-07 benchmark measurements include in situ phenomena during the laser pad process and ex situ characterization of the 3D surface topography and the pad cross sectional geometry and microstructure. The measurement methods include:

In situ measurements during the build

- In situ thermography to measure the location-dependent cooling rates of the solid material immediately after solidification. This also includes the time a specific location was above melting (the midpoint between solidus and liquidus). Thermography was collected for samples with and with powder. However, challenge problems are only associated with bare plate samples.

Ex situ measurements

- Focus variation microscopy was used to measure the 2.5D surface topography. These measurements were performed for all samples; however, the challenge is only based on a fixed laser turnaround time with different powder layer thicknesses.
- 2D cross sections were measured using a combination of SEM and optical microscopy. SEM measurements were only performed on a smaller subset of samples.

3.1 In situ thermography

Methods for defining and extracting the location-specific 'time above melt' and 'solid cooling rate' from thermographic data will largely follow those from the prior AM-Bench: AMB2022-01 measurement and challenge description [5]. Certain assumptions regarding material emissivity, and liquidus/solidus temperatures will be made, as well as various data filtering or processing of the thermographic image data, with the aim of providing the most accurate measurement possible. It is also recognized that there are numerous potential algorithms for defining and calculating 'cooling rate' from thermographic measurements or AM simulation results. Nevertheless, the following definition is designed, not necessarily to best represent thermal features directly relatable to other phenomena (e.g., thermal energy accumulation, or microstructure evolution), but to provide the simplest and most unambiguous definition for modelers to derive and compare.

The important parameters for the analysis are 1) the effective emissivity value of $\epsilon \approx 0.5$ derived from prior AMB2022-03 measurements, 2) the assumed IN718 solidus temperature of 1260 °C, liquidus temperature of 1336 °C, and mid-point of 1298 °C, and 3) the temperature range of 110 °C below solidus temperature to define the solid cooling rate. It is anticipated that modelers submitting results to CHAL-AMB2025-07-PCRTAM will follow similar algorithms and definition of time above melt (TAM) and solid cooling rate (SCR) as described below. However, modelers are encouraged to test or implement any variation they determine as more appropriate (e.g., using a different solidus temperature), and discuss with fellow modelers and metrologists at the AM-Bench conference.

3.1.1 In-situ time above melt

The following algorithm is used to calculate 'time above melt' (t_{TAM}) for each pixel within the field of view of thermographic video data:

A. Convert thermal video to temperature utilizing assumed $\epsilon = 0.5$, resulting in temperature vs. time for each pixel (x_i,y_j) or $T(x_i,y_j,t)$.
B. Perform spatter removal algorithm (if necessary) and thresholding (to be detailed in later publications).
C. For each pixel (x_i,y_j):
    a. Extract temperature vs. time profile, $T(x_i,y_j, t)$
    b. Identify all timepoints where $T(x_i,y_j, t) = 1298$ °C (or the assumed mid-point between liquidus and solidus temperature), by finding the intersections.
    c. Identify the maximum time period, $\max(\Delta t_i)$ where **$T(x_i,y_j, t) > 1298$ °C**. Store as $t_{TaM}(x_i,y_j)$.
    d. If no $t_{TaM}(x_i,y_j)$ is identified, then store as 'not a number' $t_{TaM}(x_i,y_j)$ = NaN, or reject this pixel from further analysis.

To clarify this process, example pixel time vs. temperature data are shown in Figure 7. This figure also shows the maximum time period that a pixel is above 1298 °C, which defines it's 'time above melt' value.

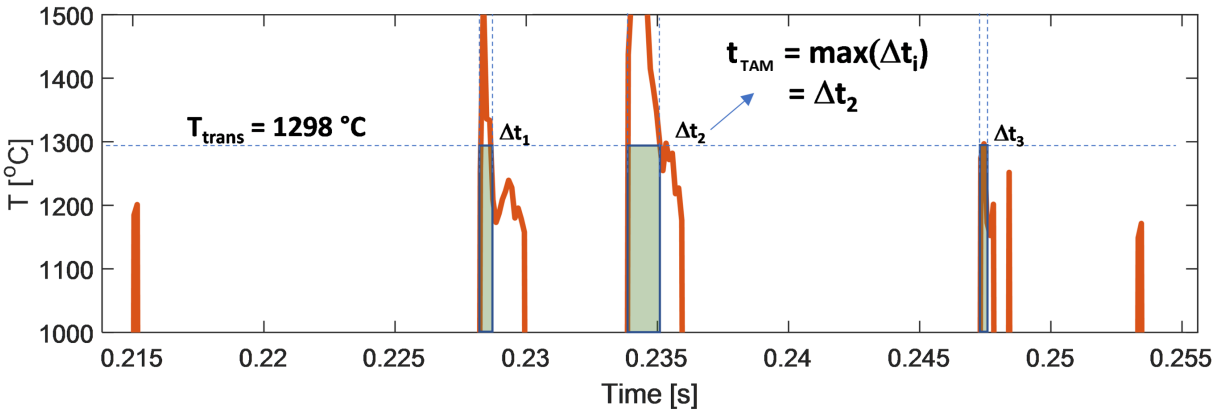

Figure 7. Schematic algorithm for calculating cumulative 'Time Above Melt' (TAM) for an individual pixel's temperature-time history.

3.1.2 In-situ solid cooling rate

The cooling rate, $\Delta T/\Delta t$, will be based on linear interpolation of the temperature vs. time for each pixel, $T(x_i,y_j,t)$, during **the same temperature peak that 'time above melt' was calculated**. The ΔT is between the assumed solidus temperature $\mathbf{T_{solidus} = 1260\ °C}$, and 110 °C below, resulting in fixed $\mathbf{\Delta T = 110\ °C}$. Therefore, the objective is to identify the time span $\mathbf{\Delta t = t_{1260} - t_{1150}}$, where t_{1260} is the time where the temperature-time curve intersects T = 1260 °C, and t_{1150} where it intersects T = 1150 °C.

The following algorithm is used to extract solid cooling rate from the 3D build thermographic data:

A. Convert thermal video to temperature utilizing assumed $\epsilon = 0.5$, resulting in temperature vs. time for each pixel (x_i,y_j) or $T(x_i,y_j,t)$.
B. Perform spatter removal (if necessary), algorithm to be detailed in later publications.
C. For each pixel (x_i,y_j):
    a. Extract temperature vs. time profile, $T(x_i,y_j,t)$
    b. Identify nominal time period when 'time above melt' is defined (See Figure 7)
    c. Identify $\mathbf{t_{1260}}$, where $T(x_i,y_j,t) = 1260$ °C (or the assumed solidus), by finding the intersection
    d. Identify $\mathbf{t_{1150}}$, where $T(x_i,y_j, t) = 1150$ °C, or 110 °C below the assumed solidus.
    e. Calculate $\mathbf{\Delta t = t_{1260} - t_{1150}}$
    f. Calculate $SCR(x_i,y_j) = \Delta T/\Delta t = (110\ °C)/\Delta t$, and store the value
    g. If no SCR is identified, then store as 'not a number' $SCR(x_i,y_j) = NaN$, or reject this pixel from further analysis.

To clarify this process, an example pixel's time vs. temperature data and Δt are shown in Figure 8.

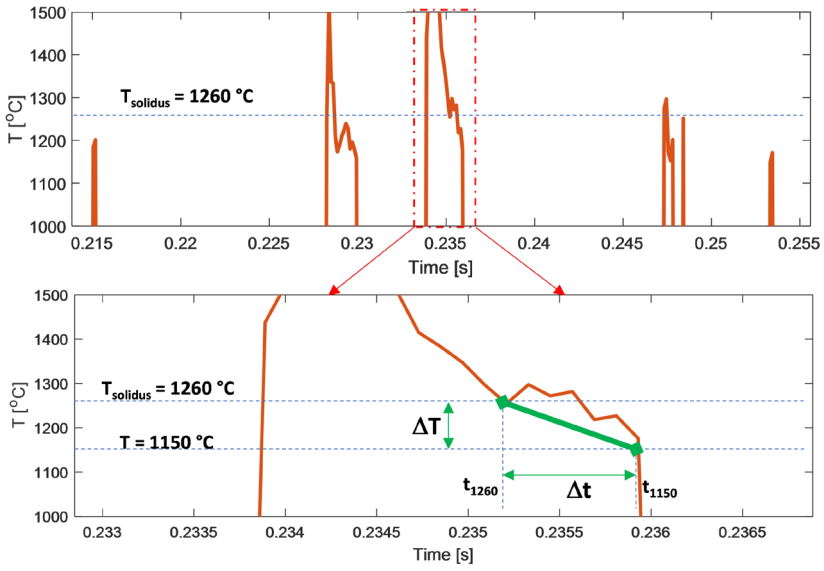

Figure 8. Calculation of 'Solid Cooling Rate' from temperature-time profiles of example pixel. Top image shows an expanded view of the pixel temperature peaks, and the bottom image demonstrates calculation of Δt based on the same temperature spike used for 'time above melt'.

3.2 Surface topography

Topographical height maps for each sample were acquired using an Alicona InfiniteFocusXL200 G5 focus variation microscope equipped with a 20X objective, providing a lateral resolution of 2.9 µm and vertical resolution of 0.06 µm. The datasets were processed using MountainsMap (v10.0) and Python (3.10). Figure 9 shows the specific regions of the samples that were used to measure the root-mean-square surface roughness (*Sq*) and fused layer thickness. Areal based surface evaluation areas are denoted as A1, A2, A3, A4, and profile-based surface evaluations are denoted as P1, P2, P3, P4. Table 9 provides written descriptions of the size and location of each evaluation area or profile used to determine surface roughness or the fused layer thicknesses for the 5 mm × 5 mm and 5 mm × 1 mm pads.

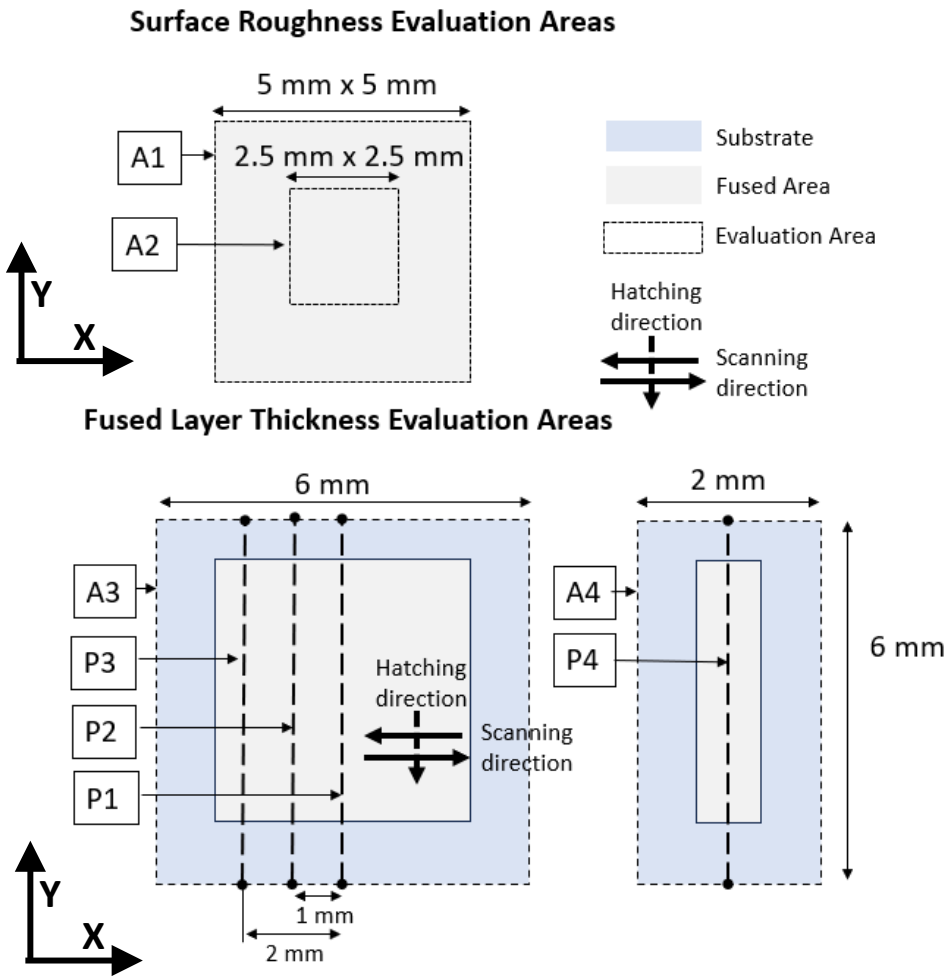

Figure 9. Areal and profile surface evaluations of 5 mm × 5 mm pad (left) and 5 mm × 1 mm pad (right) used to measure root-mean-square surface roughness (Sq) and fused layer thickness. The X and Y directions refer to the machine coordinate system. P1 and P4 are centerlines.

Table 9. Descriptions of each evaluation area or profile used to calculate root-mean-square surface roughness (Sq) or fused layer thickness.

Callout	Description
A1	5 mm × 5 mm evaluation area containing the 5 mm × 5mm pad used to measure root-mean-square height (*Sq*)
A2	2 mm × 2 mm evaluation area located at the center of the 5 mm × 5mm pad used to measure root-mean-square height (*Sq*)
A3	6 mm × 6 mm evaluation area containing the 5 mm × 5mm pad used to measure fused layer thickness

P1	6 mm profile of the 5 mm × 5 mm pad located at the center line of the pad used to measure fused layer thickness
P2	6 mm profile of the 5 mm × 5mm pad located 1 mm left of the center line of the pad used to measure fused layer thickness
P3	6 mm profile of the 5 mm × 5 mm pad located 2 mm left of the center line of the pad used to measure fused layer thickness
P4	6 mm profile down the center of the 5 mm × 1 mm pad used to measure fused layer thickness
A4	6 mm × 2 mm evaluation area containing the 5 mm × 1 mm pad used to measure fused layer thickness

After removing tilt from evaluation areas A1 and A2, *Sq* was calculated according to ISO 25178-2 [6] given by Equation 1. *Sq* is equivalent to the standard deviation of heights within the definition area.

$$Sq = \sqrt{\frac{1}{A}\iint_{\mathrm{A}} z^2(x,y)dxdy} \qquad \text{Equation 1}$$

Figure 10 illustrates how the fused layer thickness is calculated for evaluation area A3. The same methodology is applied to evaluation area A4 and 2D profiles (P1, P2, P3 and P4). Figure 10c shows a histogram of the z-height values for the surface evaluation area in Figure 10b after form removal. Form removal consisted of fitting a least-squares plane to the data within the substrate regions and subtracting the plane from the evaluation area, making the mean of the substrate topography z ≙ 0. The bin size used for the histogram is between 0.1 µm and 1 µm (note: the optimal bin size may need further adjustment). The fused layer thickness is defined as the difference between the modes of the height distributions within the substrate and the fused area (i.e., the mode of the fused area minus the mode of the substrate). If a significant discrepancy is observed between repeat samples or more than two peaks (modes) are present, the mode or height value that best agrees with the qualitative estimate shown in Figure 10a is selected.

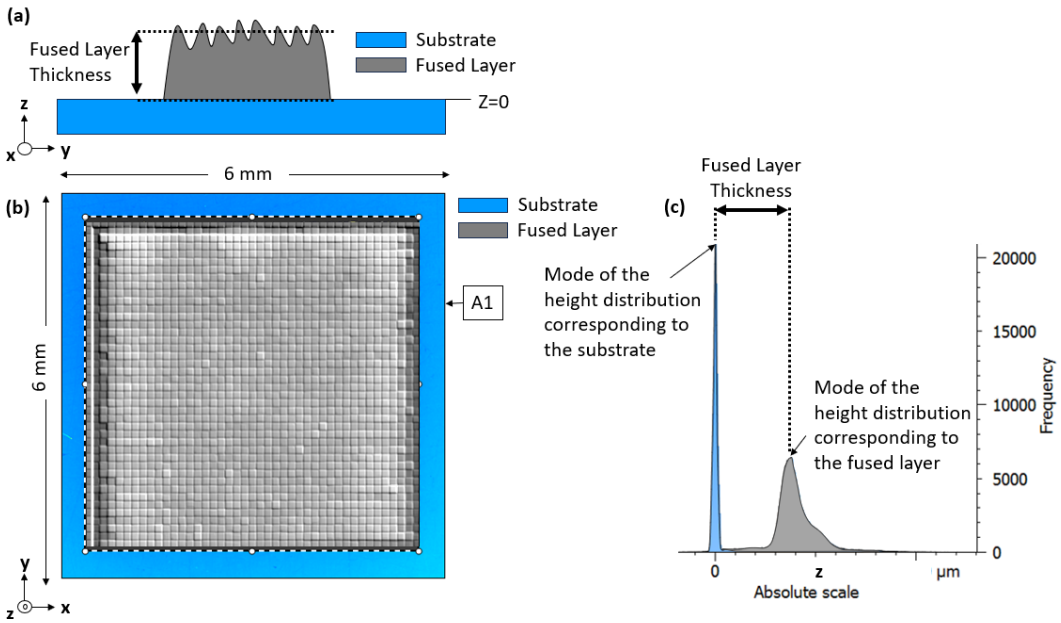

Figure 10. (a) Example of a qualitative measurement of fused layer thickness. (b) Example evaluation area and (c) corresponding quantitative measurement of fused layer thickness based on evaluation area A1.

3.3 Optical Microscopy

3.3.1 Cross-section positions

Samples were cross sectioned using a multi-step process, which included grinding each sample by hand to specific fiducial markers to enable measurements at the same position for repeat pad scans. The cross-section position uncertainty was determined to be ± 75 µm (p = 95%) using optical microscopy and the presence of fiducial markers. The cross-sections were also perpendicular to the laser scan direction with a maximum deviation angle of 1°. The cross-section positions are based on the measured pad centroids and the programmed pad geometry (i.e., 5 mm × 5 mm and 5 mm × 1 mm). The centroids were determined through image segmentation of optical micrographs. Figure 11 shows an example result with the pad geometry boxes (red lines) centered on the segmented area (white region). Visually this also shows the pad geometry reasonable agrees with the programmed geometry (see the scan strategy described in Figure 4).

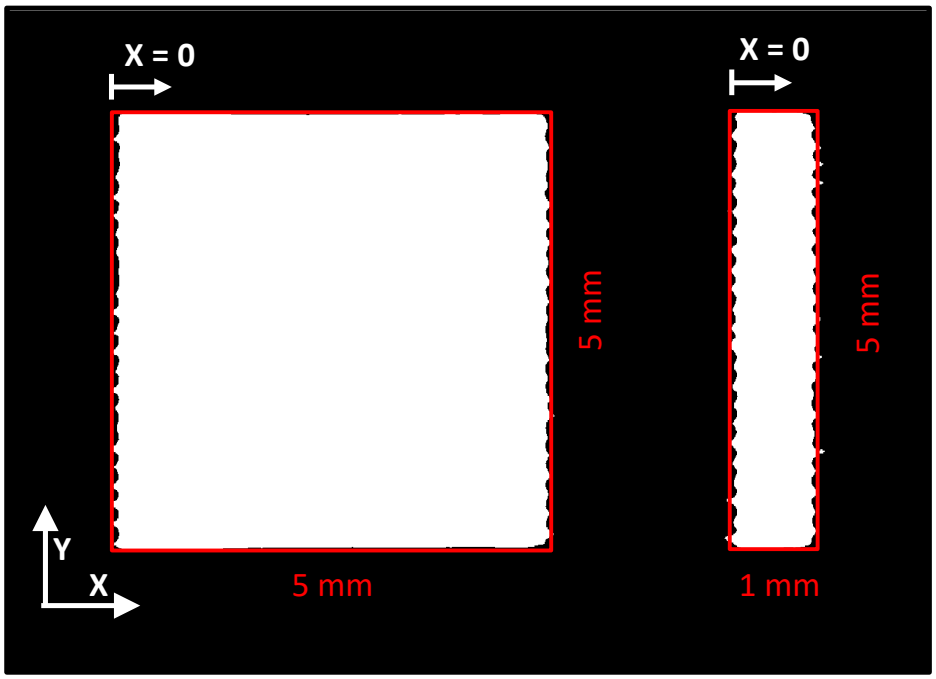

Figure 11. Segmented image to determine the pad centroid. Red boxes are the prescribed pad geometry centered on the pads shown in white. The relative position of cross-sections is referenced to the left edge of the pad red boxes noted with X = 0.

3.3.2 Melt pool geometry definitions.

Here we define several measurands listed in Table 10 and schematically shown in Figure 12 for pad scans. The initial plate surface is used as a reference line. There are 45 tracks in each pad leading to 45 bead height, depth, and width measurements and 44 overlap depth and overlap width measurements. Melt pool measurements are made on solidified melt pools; this is not to be confused with in-situ measurements of the metal still in liquid phase. Measurements were made using a combination of ImageJ (v1.54f) and MATLAB (v2024a).

Table 10. List of cross-sectional melt pool measurands. See Figure 12 for schematics.

No.	Measurand Name	Variable	General Description
1	Bead height	b	Vertical distance from the initial surface to the top of each melt pool.
2	Depth	d	Vertical distance between the initial surface and the bottom of each melt pool.
3	Overlap depth	d_o	Vertical distance from the initial surface to the lowest intersection between two consecutive melt pools.
4	Width	w	The horizontal distance from the deepest point to the trailing edge of a melt pool.
5	Overlap Width	w_o	The horizontal distance between the trailing edges of two consecutive melt pools.
6	Solidified layer area	n/a	Area of solidified material above the initial surface.
7	Dilution layer area	n/a	Area of solidified material below the initial surface.

8	Track 45 melt pool micrograph	n/a	A binary image with 1 for the melt pool and 0 elsewhere. The pixel size and the pixel row for the initial surface shall be provided. This is used for melt pool morphological comparisons.

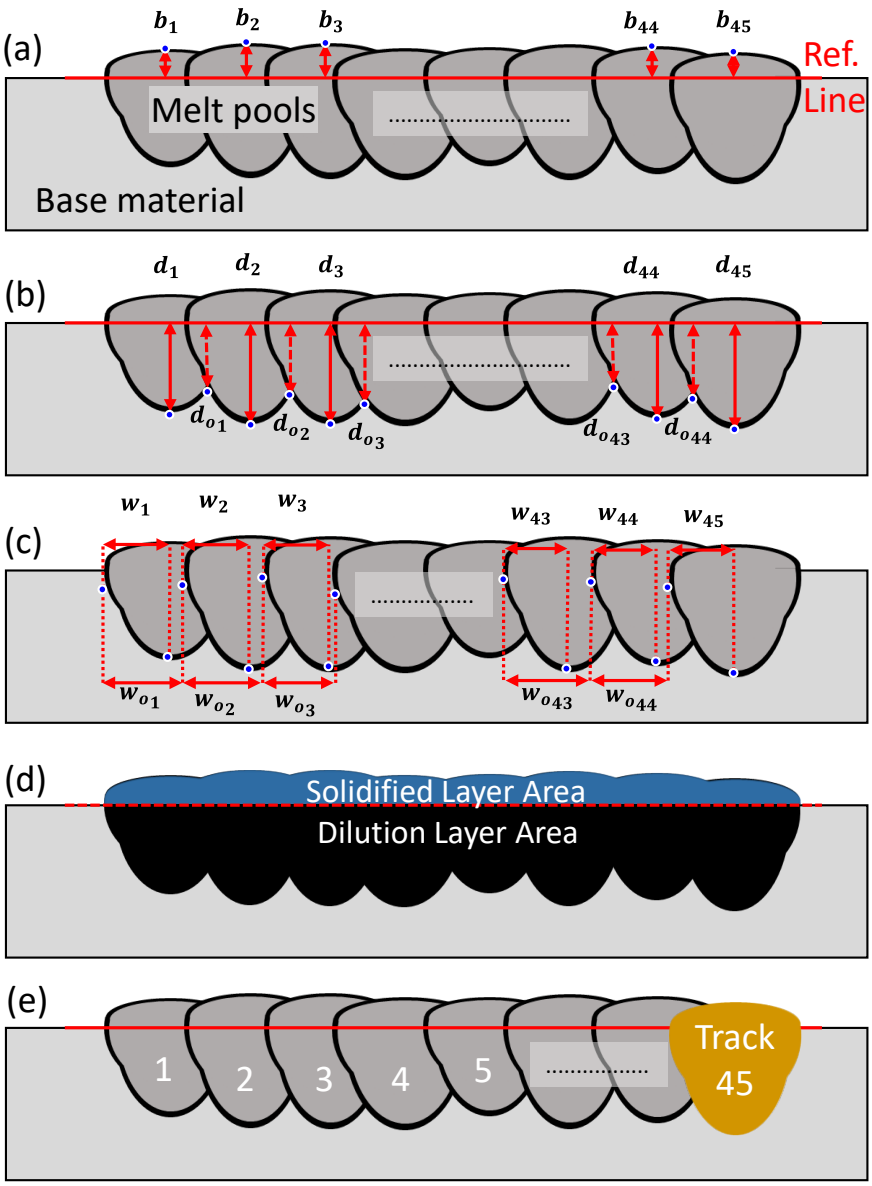

Figure 12. Schematic representation of cross-sectional melt pool measurands: (a) bed height, (b) depth and overlap depth, (c) width and overlap width, (d) solidified and dilution layer areas, (e) final track melt pool image. See Table 10 for further description.

3.4 Scanning Electron Microscopy (SEM)

SEM micrographs and Electron backscatter diffraction (EBSD) maps will be collected for select conditions and select regions of interest to provide microstructure information for the pad experiments. Specific

measurement procedures are not available currently. There is no challenge problem associated with these measurements so the data will be released in a timely manner after challenge problem cycle.

4 Description of Benchmark Challenge Problems

The following sections describe how submissions will be evaluated and compared against measurement results. Please use the templates provided for each challenge.

4.1 CHAL-AMB2025-06-PMPG

Modelers are to calculate the average bead height, depth, overlap depth, and width for each pad cross-section and report these values in micrometers with one decimal value. There are 3 powder layer thicknesses (0 µm, 80 µm, 160 µm) and three cross-sections (5 mm pad at 0.460 mm, 5 mm pad at 2.545 mm, 1 mm pad at 0.556 mm). This results in a table with 4 × 3 × 3 = 36 entries for the measurands above. In addition, modelers are to calculate the solidification layer area and dilution layer area for each cross-section and report these values to the nearest µm². This results in an additional 2 × 3 × 3 = 18 entries. Lastly, modelers are to calculate the bead height, depth, and width for the first 5 tracks for the 160 µm layer thickness, 5 mm pad at 2.545 mm. This is a second table with an additional 15 entries. A submission template can be found in the calibration dataset (§5). Modelers will be judged on the average of the difference between the 69 predictions (P) and measurements (M) in Equation 2. Awards will be made at the discretion of the AM Bench organizing committee.

$$\Delta_{06_{PMPG}} = \frac{1}{69}\sqrt{\sum_{i=1}^{69}\left(\frac{P-M}{M}\right)^2} \qquad \text{Equation 2}$$

4.2 CHAL-AMB2025-06-PST

Modelers are to calculate the fused layer thickness and root-mean-square-height ($\boldsymbol{S_q}$) as described in §3.2. Qualitative or quantitative assessments of fused layer thickness are acceptable. If the procedure described in §3.2, Figure 10 is used to obtain values, modelers should ensure meshing is nominally uniform to avoid oversampling certain regions of the surface topography for the histogram evaluation. Table 11 provides an empty table of the results that modelers will submit for evaluation. The submission template with this table and additional information is provided in the calibration dataset (see §5).

Table 11: Summary of predictions for the challenge. Please use the template document provided in the calibration dataset (§5). See Table 10, Figure 9, and Figure 10 for schematics and descriptions.

	5 mm x 5 mm pad						5 mm x 1 mm pad	
	A1	A2	A3	P1	P2	P3	P4	A4
Powder Layer Thickness (µm)	Root mean square height (Sq) µm	Root mean square height (Sq) µm	Fused Layer Thickness (µm)	Fused Layer Thickness (µm)	Fused Layer Thickness (µm)	Fused Layer Thickness (µm)	Fused Layer Thickness (µm)	Fused Layer Thickness (µm)

0								
80								
160								

Scoring will be based on Equation 3, which is the average percentage difference between predictions (x_{pred}) and measurements (x_{meas}). Awards will be made at the discretion of the AM Bench committee.

$$Avg.\%\ Difference = \frac{\sum_{i}^{24} \frac{|x_{pred} - x_{meas}|}{\frac{1}{2}(x_{pred} + x_{meas})}}{24} \quad \text{Equation 3}$$

4.3 CHAL-AMB2025-07-PCRTAM

Modelers are to calculate 'time above melting' and 'solid cooling rate' as close as possible to the definition or algorithm described in §3.1. Modelers should calculate the following statistical features:

- Number of pixel/element/nodes that TAM is interrogated from model results (e.g., sample size)
- Mean of all pixel/element/nodal TAM values
- Median of all pixel/element/nodal TAM values
- Standard deviation of all pixel/element/nodal TAM values
- Number of pixel/element/nodes that SCR is interrogated from model results (e.g., sample size)
- Mean of all pixel/element/nodal SCR values
- Median of all pixel/element/nodal SCR values
- Standard deviation of all pixel/element/nodal SCR values

Modelers shall provide tabulated full $t_{TaM}(x_i,y_j)$ and $SCR(x_i,y_j)$ array data to AM-Bench organizers, alongside the above-mentioned statistical features. The full array data will be used for more comprehensive statistical comparison to thermographic results (e.g., Kolmogorov–Smirnov test). Additionally, modelers should supply pictures and/or a brief description of the model formulation. See the template in the calibration data set (§5).

Note that it is not expected that the AM simulation outputs exactly replicate the temporal, spatial, or temperature resolution or range of the thermographic imaging system, and model formulations may utilize certain approximations that render results outputs that are less-physically equivalent to the thermographic measurements described in §3.1. Therefore, participants should consider the following:

A. The number of pixels/elements/nodes may vary but should **not be more than N = 1E6** (e.g., equivalent to approx. 5 µm pixel size). Additionally, values should be extracted **from a uniform grid** on the surface of each layer so as not to weight the statistics towards certain regions.

B. In calculating the above statistical features, modelers should reject values outside the measurable/calculable TAM and SCR results (e.g., reject '0' values). Modelers may also wish to reject statistical outliers.

C. Depending on the model formulations, modelers may also consider testing or utilizing different algorithms or definitions of 'time above melt' (e.g., using a different threshold temperature). However, for the modelling challenge, model results will be compared against measurement results as described in §3.1. *Only one entry from each participating research group will be used for the challenge judging.*

Awards will be made at the discretion of the AM Bench committee.

4.4 CHAL-AMB2025-07-PMPG

Modelers are to calculate the average bead height, depth, overlap depth, and width for each pad cross-section and report these values in micrometers with one decimal value. There are 2 laser turnaround times (0.75 ms, 5.0 ms) and three cross-sections (5 mm pad at 0.460 mm, 5 mm pad at 2.545 mm, 1 mm pad at 0.556 mm). This results in a table with 4 × 2 × 3 = 24 entries for the measurands above. In addition, modelers are to provide a binary image of the last melt pool (track number 45) for each cross-section, the pixel size in micrometers, and pixel position (pixel number) of the initial surface so that the morphology can be compared (see Figure 13). The image format should be a .tif with no compression. Images with a pixel scale that are different from 0.069 µm/pixel will either be up sampled or down sampled in order to compare with the measurement result. The predicted and measured track 45 melt pools will be aligned using the initial surface for the y-position and the area centroid for the x-position followed by a difference calculation. This results in 1 × 2 × 3 = 6 additional entries. A submission template can be found in the calibration dataset (§5). Modelers will be judged on the aggregate of the difference between the 30 predictions (P) and measurements (M) in Equation 4. Awards will be made at the discretion of the AM Bench committee.

$$\Delta_{07_{PMPG}} = \frac{1}{30}\sqrt{\sum_{i=1}^{30}\left(\frac{P-M}{M}\right)^2} \qquad \text{Equation 4}$$

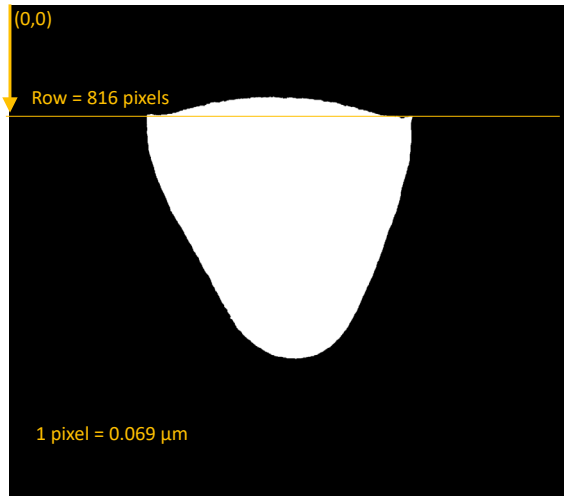

Figure 13. Example binary image of final melt pool with schematic showing the origin is in the top left corner, the reference surface is 816 pixels from the origin, and the scale is 1 pixel = 0.069 µm. Submissions should provide an image (.tiff) without annotations. The reference surface pixel number and scale should be provided in the template table.

5 Calibration Dataset

The calibration data, beyond what is provided in this document, are provided at the following DOI: https://doi.org/10.18434/mds2-3707. This includes a ReadMe file with a data manifest. A basic lookup table is provided in Table 12 for easy reference.

Table 12. Description of calibration data

Data Description	Path
IN718 plate material specification	Plate\
IN718 powder specification	PowderFeedstock\
Powder size measurements	PowderFeedstock\PSD\
Powder layer images	SpreadLayerImages\
Singe track melt pool micrographs and measurements	MeltPoolCrossSection\
Scan path measurements	ScanStrategy\
Submission templates	SubmissionTemplates\

6 References

[1] ASTM (2021)– *F3055-14a Standard Specification for Additive Manufacturing Nickel Alloy (UNS N07718) with Powder Bed Fusion* (ASTM International, West Conshohocken, PA).

[2] Deisenroth D, Mekhontsev S, Grantham S (2025) Design and Calibration of the Fundamentals of Laser-Matter Interaction (FLaMI) Powder Bed Fusion Testbed at NIST. (National Institute of Standards and Technology).

[3] Kirillov A, Mintun E, Ravi N, Mao H, Rolland C, Gustafson L, Xiao T, Whitehead S, Berg AC, Lo W-Y (2023) Segment anything. *Proceedings of the IEEE/CVF International Conference on Computer Vision*, pp 4015-4026.

[4] Weaver JS, Deisenroth D, Mekhontsev S, Lane BM, Levine LE, Yeung H (2024) Cross-Sectional Melt Pool Geometry of Laser Scanned Tracks and Pads on Nickel Alloy 718 for the 2022 Additive Manufacturing Benchmark Challenges. *Integrating Materials and Manufacturing Innovation* 13(2):363-379. https://doi.org/10.1007/s40192-024-00355-5

[5] (2022) *AMB2022-01 Benchmark Measurements and Challenge Problems* (NIST). Available at https://www.nist.gov/ambench/amb2022-01-benchmark-measurements-and-challenge-problems.

[6] ISO (2021)– *ISO 25178-2:2021 Geometrical product specifications (GPS) - Surface Texture: Areal - Part 2: Terms, definitions, and surface texture parameters.*

Disclaimers

The National Institute of Standards and Technology (NIST) uses its best efforts to deliver high-quality copies of the AM Bench database and to verify that the data contained therein have been selected on the basis of sound scientific judgment. However, NIST makes no warranties to that effect, and NIST shall not be liable for any damage that may result from errors or omissions in the AM Bench databases.

Certain commercial equipment, instruments, or materials are identified in this paper in order to specify the experimental procedure adequately. Such identification is not intended to imply recommendation or endorsement by NIST, nor is it intended to imply that the materials or equipment identified are necessarily the best available for the purpose.